PCCP

ROYAL SOCIETY OF CHEMISTRY

PAPER

View Article Online
View Journal

Cite this: DOI: 10.1039/d3cp05415b

Ion mobility calculations of flexible all-atom systems at arbitrary fields using two-temperature theory†

Farah Mubas-Sirah, ‡[a] Viraj D. Gandhi, ‡[ab] Mohsen Latif,[a] Leyan Hua,[a] Amirreza Tootchi[a] and Carlos Larriba-Andaluz*[a]

Received 7th November 2023,
Accepted 5th January 2024

DOI: 10.1039/d3cp05415b

rsc.li/pccp

Ion mobility spectrometry (IMS) separates and analyzes ions based on their mobility in a gas under an electric field. When the field is increased, the mobility varies in a complex way that depends on the relative velocity between gas and ion, their electrostatic potential interactions, and the effects from direct impingement. Recently, the two-temperature theory, primarily developed for monoatomic ions in monoatomic gases, has been extended to study mobilities at arbitrary fields using polyatomic ions in polyatomic gases, with some success. However, this extension poses challenges, such as inelastic collisions between gas and ion and structural modifications of ions as they heat up. These challenges become significant when working with diatomic gases and flexible molecules. In a previous study, experimental mobilities of tetraalkylammonium salts were obtained using a FAIMS instrument, showing satisfactory agreement with numerical two-temperature theory predictions. However, deviations occurred at fields greater than 100 Td. To address this issue, this paper introduces a modified high-field calculation method that accounts for the structural changes in ions due to field heating. The study focuses on tetraheptylammonium (THA^+), tetradecylammonium (TDA^+), and tetradodecylammonium ($TDDA^+$) salts. Molecular structures were generated at various temperatures using MM2 forcefield. The mobility was calculated using IMoS 1.13 with two-temperature trajectory method calculations up to the fourth approximation. Multiple effective temperatures were considered, and a linear weighing system was used to create mobility *vs.* reduced field strength plots. The results suggest that the structural enlargement due to ion heating plays a significant role in mobility at high fields, aligning better with experimental data. FAIMS' dispersion plots also show improved agreement with experimental results. However, the contribution of inelastic collisions and energy transfer to rotational degrees of freedom in gas molecules remains a complex and challenging aspect.

Introduction

Ion mobility spectrometry (IMS) is a valuable analytical technique used in various fields of science, including chemistry, environmental science, and security applications.[1–4] It allows users to separate and study ions based on their mobility in a gas under the influence of an electric field.[5–7] A key element in mobility calculations involves grasping the impact that relative velocities between gas and ions have on the ion's mobility behavior.[8–10] Higher fields imply larger average relative velocities, which in turn affect mobility through two competing effects: (a) direct collisions with the ion are stronger causing the ion to slow down and (b) gas residence time is lower, which affects capture and grazing trajectories reducing the overall momentum transfer.[11–13] As such, the ion mobility may increase or decrease with the field, leading to the typical A, B, C or D mobility types. These behaviors are thoroughly explained elsewhere and are summarized in the ESI.†[9,11,14]

Aside from slowing the ions down, direct collisions also increase the temperature of the ion.[7,15,16] While at low electric fields, it is typical to assume that the ion has the same temperature as the gas bath,[5] an increase in the electric field ultimately results in raising the ion's temperature over that of the gas. This dynamically acquired temperature is referred to as the effective temperature (T_{eff}) of the ion.[8,13,17,18] While it is conceptually easy to understand that a body would heat in the presence of gas and high acceleration, how the heating occurs

[a] Department of Mechanical Engineering, Indiana University – Purdue University Indianapolis, Indianapolis, IN, USA. E-mail: clarriba@iupui.edu
[b] Department of Mechanical Engineering, Purdue University, West Lafayette, IN, USA

† Electronic supplementary information (ESI) available: IMoS113_SI.docx and IMoS UserManual_113.docx. See DOI: https://doi.org/10.1039/d3cp05415b

‡ V. D. G. and F. M. S. contributed equally.

is rather complicated.[8,17–20] Its theoretical understanding has been a subject of study for more than a century, with theories such as the two-temperature approximation which, as its name suggests, assigns a different temperature to the ion and gas. In the two-temperature theory, intended for monoatomic ions in monoatomic gases and elastic collisions, the gas-ion pair interacts at a higher relative energy, which affects the drift velocity of the ion, and hence the mobility. This relative energy is equated directly to the effective temperature of the system and this equality, in its first approximation, is known as Wannier's equation.[21] The effect is however not straightforward, as the increase in temperature also affects mobility indirectly by, for example, increasing the diffusion of the ion – *i.e.*, the width of the ion velocity distribution.[8] For a comprehensive introduction to the theory, one can look at the multiple works of Mason and Viehland in the late 1900s.[8,18,22–26]

More recently, the two-temperature theory has been employed to study polyatomic ions in polyatomic gases quite successfully,[19,27] including our own description of how to obtain the matrix elements up to the fourth approximation.[11,13,17] Two caveats must be noted before the technique can be used for polyatomic entities. The first caveat is that the two-temperature assumption that the collisions between gas and ion are elastic must be relaxed as energy can be lost into the internal degrees of freedom of the gas and ion.[2,28–31] The second is that as ions heat up, their geometry might vary, leading to structural modifications that affect the overall mobility.[32,33] Neither of these issues seems significant for monoatomic gases (*e.g.*, helium) and small rigid ions, leading to numerical results in good agreement with experimental results even for very large fields.[13,25,26] However, a deviation of the theory from experiments is expected when using diatomic gases and flexible molecules.[29,30,34]

In a previous manuscript,[35] we obtained the experimental mobilities of tetraalkylammonium salts at arbitrary fields using a High Field Asymmetric Waveform Ion Mobility Spectrometry (FAIMS)[9,36–39] instrument coupled to a Differential Mobility Analyzer (DMA).[40,41] The experimental results were tested against our numerical two-temperature theory prediction. Results were satisfactory for up to 100 Td, but deviated at higher fields. We posited that the deviation was partially due to the inelasticity of the collisions and partially due to the enlargement of the structures. However, no attempt was made to differentiate the two. To resolve the issue, in this manuscript, we have modified our high-field calculations to allow multi-structure two-temperature mobility calculations as a function of the field. The calculation package has been optimized and added to our suite of algorithms and calculates mobility *vs.* reduced field strength (field over concentration E/n) and dispersion plots in record time.[42] Results show that the mobility is reduced by the enlargement of the structure due to the field heating, better aligning numerical results with their experimental counterpart.

Methods

Tetraheptylammonium (THA^+), Tetradecylammonium (TDA^+), and Tetradodecylammonium ($TDDA^+$) salts were modeled using Chem3D Pro.[43] MM2 was used to provide molecular structures of the salts at different temperatures.[44] Three different structures at three different temperatures (295 K, 390 K, and 480 K for $TDDA^+$; 295 K, 400 K, and 500 K for TDA^+; 295 K, 460 K, and 600 K for THA^+) were chosen. The models were initially minimized and equilibrated at 295 K. After equilibration, the models were heated up from 295 K to the desired effective temperature and then sampled at that temperature for 10 ns. While many structures were obtained at every given temperature, only one average structure was used for the mobility calculation for each salt. This process was based on the understanding that at higher temperatures, molecules can more easily overcome barriers to isomerization, leading to the presence of multiple isomers or structural variants. However, accounting for the mobility of every possible isomer structure is rather difficult, particularly for the case of the dynamic isomerization between conformers induced by collisions.[45] Therefore, selecting a structure that represents the mean mobility of many different isomers provides a practical and effective approach to our mobility calculations.[46–51] The result from choosing similarly averaged structures does not affect the mobility significantly. Candidate structures at the base

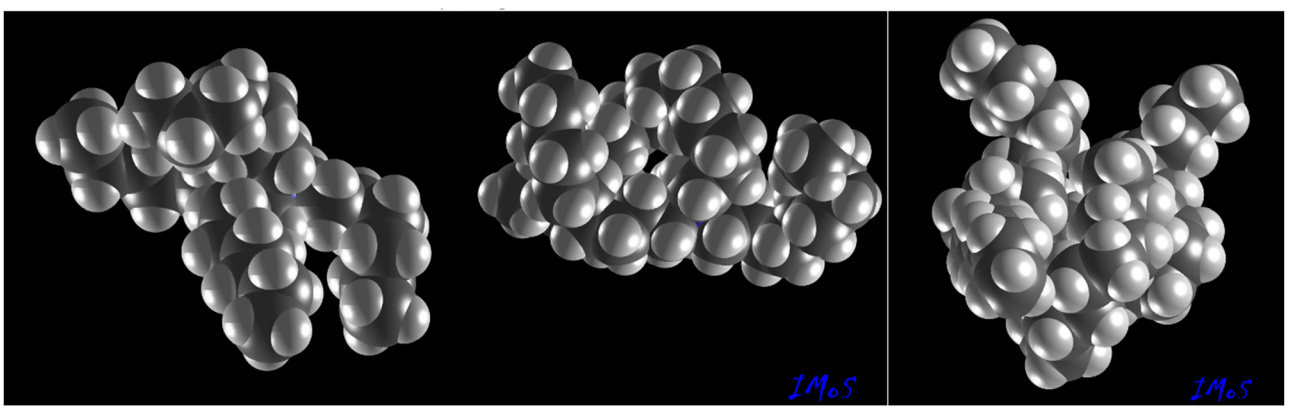

Fig. 1 Candidate structures of tetraalkylammonium salt at 295 K for THA^+ (left), TDA^+ (middle) and $TDDA^+$ (right). The coordinates of the atoms are available in the ESI.†

temperature of 295 K are shown in Fig. 1 and the atomic locations are also tabulated in the ESI† for all temperatures used.

IMoS version 1.13 was chosen for the two-temperature high-field calculations and the mobility, and CCS were calculated up to the fourth approximation. The way the two-temperature theory calculations are performed was described previously[11,52] and will not be depicted thoroughly in this work. Briefly, series solutions of the moments of the Boltzmann equation are obtained as closed quadratures that are functions of complex coefficients that are known as matrix elements. These matrix elements are functions of collision integrals computed *via* trajectory calculations incorporating ion-induced dipole potentials and van der Waals forces, using the Trajectory Method Lennard-Jones (TMLJ) approach. The TMLJ method was favored in this study over the quadrupole potential-inclusive TMLJ qpol method, as it offers comparable accuracy with increased computational efficiency. For both sets of trajectory calculations, TMLJ and TMLJ qpol, the methodological refinements in IMoS 1.13 have resulted in 50% faster calculations compared to IMoS 1.12, as shown in Fig. 2. Remarkably, the 1.13 version approximately takes 34 minutes to calculate for over 20 000 atoms using 12 cores. Using 32 cores, it takes approximately 14 minutes. The trajectory method calculations are then employed to calculate the collision integrals, the matrix elements required to achieve the fourth approximation, and ultimately the mobility as a function of the reduced field strength.

To obtain the ion mobility *vs.* E/n plot that includes the effect of the structural changes, the mobilities of the temperature variant structures were first calculated at various effective temperatures using IMoS.[11,42,53] The resulting mobilities were then combined using linear weighted averages to generate a singular mobility plot as a function of the reduced field. Only the two closest structures to a particular effective temperature were used in the weighing. The resulting mobility to reduced field strength values can then be used to obtain a dispersion plot using the method shown in ref. 35 and 37. In this study, a typical bisinusoidal dispersion field was used, however, any waveform can be analyzed.[9] A thorough example explaining how these calculations are performed using IMoS 1.13 is given in the ESI† as well as the software manual. IMoS 1.13 can be downloaded from **https://www.imospedia.com**.

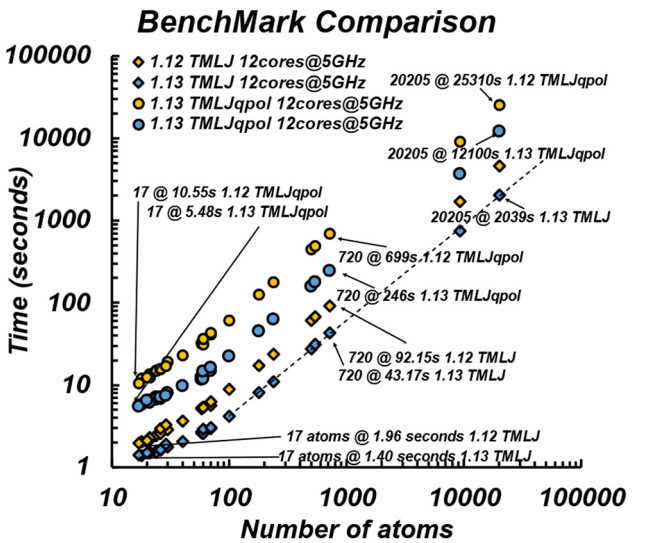

Fig. 2 Benchmark comparison in speed between IMoS v. 1.12 and IMoS v. 1.13 showcasing an increase in speed of larger than 50% in most cases.

Results and discussion

The idea that an ion can heat up as it accelerates in the presence of an electric field is not new and has been observed in multiple scenarios.[15,16,25,26,29,30,54] What is particularly pertinent is understanding the extent to which the ion heats up as a function of the imposed field and gas parameters. The development of theories like the two-temperature theory, as well as more advanced models like the three-temperature theory or Gram-Charlier theories,[24,55–57] stemmed from the need to investigate ion behavior under arbitrary fields, encompassing the influence of the field on the ion's translational energy and temperature increase due to interactions with the gas. While very promising, the two-temperature theory was originally envisioned to work for monoatomic entities, addressing the moments of the Boltzmann equation without accounting for internal degrees of freedom. As such, the two-temperature theory considered the collisions to be perfectly elastic, with energy exclusively exchanged between the translational degrees of freedom of ion and gas. However, this assumption often warrants caution when extended to polyatomic entities, as discrepancies between theoretical predictions and experimental observations may emerge, requiring suitable corrections.

To investigate this, one can refer to previously obtained experimental mobilities of tetraalkylammonium ions, measured as a function of reduced field strength with a DMA-FAIMS hybrid system in ambient air conditions.[35] Methodology of this experimental setup, detailed elsewhere,[35] involves a DMA acting as a primary filter and measuring mobility in a uniform, low electric field. FAIMS, on the other hand, creates an asymmetrical waveform between parallel plates where the ions are passing through, separating them based on the ratio of mobility at high and low field. Using this ratio and absolute mobility measured through the DMA, one can create a mobility *vs.* E/n curve using Buryakov's equation, as presented in Fig. 3.[35,37] In the same figure, we can observe over-imposed numerical results obtained through the fourth approximation of the two-temperature theory, which exhibit reasonable agreement with experiments,[17] with noticeable deviations occurring at reduced field strengths exceeding 100 Td. Notably, in all instances, the experimental data indicate lower mobilities when contrasted with the calculated values. Two potential complementary hypotheses were proposed as possibilities for the disparity.

The first hypothesis indicated that the effect was partially attributed to the non-elastic nature of the gas-ion collisions at high-fields.[2,29,58,59] Contrary to two-temperature theory assumptions of purely elastic collisions in the translational energy sense, in the context of polyatomic ions and gases, some

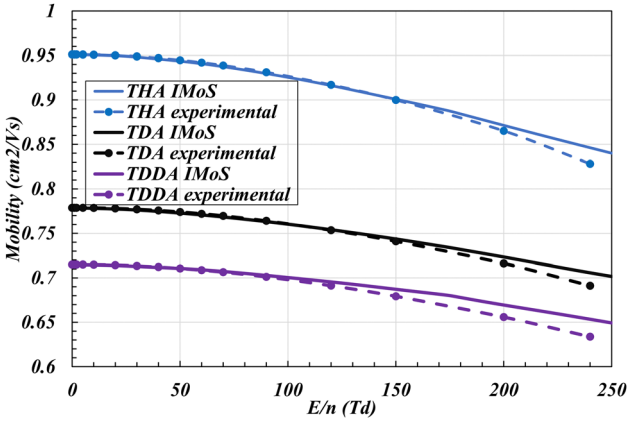

Fig. 3 Mobility as a function of reduced field strength for the three tetraalkylammonium salts: a comparison of experimental results (indicated by dashed lines and markers) and numerical simulations (represented by solid lines). Experimental data and the DFT structure to perform the mobility calculations are taken from ref. 35.

of the energy from the collision might go into the internal degrees of freedom of the ion and/or the gas. Given enough time, the energy absorbed by the ion's internal degrees of freedom lead to its equilibration at an effective temperature. Conversely, the energy transferred to the polyatomic gas' internal degrees of freedom is dispersed to other gas molecules and ultimately to the walls of the system, resulting in energy loss that cannot be equilibrated or recuperated by simple means. Quantifying this loss is a challenging task and will undoubtedly result in a different effective temperature than if only purely elastic collisions were considered. The difference between elastic effective temperature and inelastic (or true) effective temperature can be given by:[2]

$$\frac{3}{2}kT_{\text{eff}}^{\text{inel}}\left(1+\frac{m}{M}\xi\right)=\frac{3}{2}kT_{\text{eff}}^{\text{el}} \quad (1)$$

where k is the Boltzmann constant, m/M is the ratio of the mass of the gas to the mass of the ion, $T_{\text{eff}}^{\text{inel}}$ and $T_{\text{eff}}^{\text{el}}$ are the inelastic and elastic effective temperatures, and ξ is the inelasticity coefficient. While the inelasticity coefficient is analytically quite complex, one could certainly obtain it by comparing experimental and numerical results as the effective temperature can be inferred from the reduced field strength.

The second hypothesis stems from the concept that ion heating can lead to structural expansion, indicative of an increase in the average size of various isomers.[45,60] This might be particularly important in the case of long chain flexible systems like tetraalkylammonium salts.[60,61] The enlargement of the structure will reduce its mobility, agreeing with what is observed experimentally, and complementing the inelastic effects of the gas. Recreating this second effect is inherently more manageable, as it only requires Molecular Dynamics (MD) simulations to generate appropriate structures at higher temperatures to calculate mobility at higher effective temperatures. However, a critical challenge arises from the fact that the mobility calculations are optimized for the structures obtained through Density Functional Theory (DFT) calculations.[62] MD simulations tend to produce larger structures compared to their DFT counterparts, which renders them generally unsuitable for mobility calculations without careful consideration. Conversely, general DFT calculations cannot typically account for temperature variations.[63] In Fig. 3, mobility was determined using the ground state DFT structure of tetraalkylammonium salts, which is expected to yield accurate mobility at the room temperature. However, as the effective temperature of the ion increases, structural adjustments become necessary – a task that DFT cannot accommodate. It is therefore necessary to find a way that can utilize MD to generate higher temperature structures while simultaneously producing accurate mobility values. To overcome this in our study, we have opted to employ IMoS 1.13 structure reduction coefficient to provide suitable mobility and Collision Cross Section (CCS) values. The reduction coefficient uses the center of molecule and position of the atoms to compress the molecule a given percentage equivalent to the inverse of the reduction coefficient. To ensure consistency, the same reduction coefficient has been used for all the structures generated for the given salt. However, the reduction coefficient has been adjusted for each salt to match the experimental value at zero field.

To gain a comprehensive understanding of the methodology, the Tetradodecylammonium ($TDDA^+$) salt will be highlighted here. Initially, a two-temperature theory calculation using IMoS 1.13 Lennard-Jones trajectory method in Nitrogen was performed using the MD structure at the gas temperature of 295 K yielding a mobility of 0.65 $cm^2\ V^{-1}\ s^{-1}$. Given that the obtained mobility was lower than the experimental counterpart (0.715 $cm^2\ V^{-1}\ s^{-1}$),[64] the structure was scaled down using a reduction coefficient of approximately 1.13, determined by manually iterating through various values of the 'red_coef' variable in IMoS. This adjustment aimed to align the results with both experimental data and those derived from a standard DFT calculation. Subsequently, the fourth approximation to the mobility using the two-temperature theory is calculated for the three (or whatever number is chosen) structures at various effective temperatures: 295, 296, 297, 298.5, 300, 302, 305, 308, 312, 315, 320, 325, 330, 340, 350, 365, 380, 420, 470, 530, 600, 680, 770, 870, 980, and 1100 K. Notably, the effective temperatures chosen do not need to be the same as the selected temperatures for the structures (in this case 295 K, 390 K and 480 K). However, if they differ, the system will also calculate the mobility at the structure's temperature (*e.g.*, 390 K). The program then automatically chooses which effective temperatures to run for each of the structures to optimize computational time. The results, depicting the mobility as a function of reduced field strength, are illustrated in Fig. 4, with detailed tabulated information provided in the ESI.† Considering a combination of all the structures, the program employs a linear weighting system to calculate the mobility as a function of reduced field strength. While this example utilizes only three different temperatures for clarity, employing a larger number of effective temperatures together with a larger number of structures would yield more accurate results. As anticipated from the hypothesis, the resulting mobility curve exhibits a steeper slope

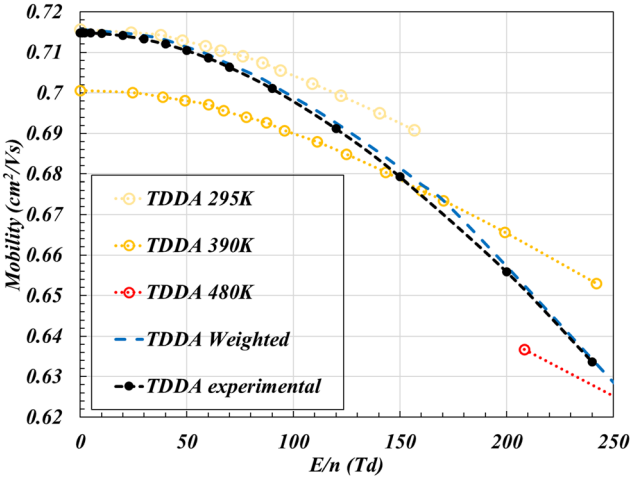

Fig. 4 Mobility as a function of reduced field strength for the $TDDA^+$ salt. Three different structures are used at different temperatures and weighted to obtain a curve that can be compared to the experimental value.

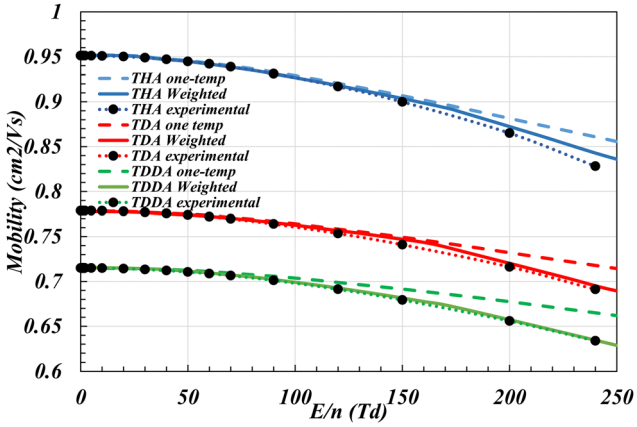

Fig. 5 Mobility as a function of reduced field strength for THA, TDA and TDDA salts. For each salt, the graph shows single structure (dashed), weighted (solid) and experimental (dotted with markers) result.

than if only the 295 K structure were used. In this specific case, it closely approximates the experimental value, albeit with the caveat that a reduction coefficient was used to initially match the zero-field value. To reiterate, the reduction coefficient is applied to compress the MD structures to match with the actual (or DFT) structures generated at different temperatures. Then, the mobility of these structures is calculated at various E/n values, and subsequently interpolated to create a continuous mobility *vs.* E/n curve. A noteworthy observation from the tabulated results is that, for the first 100 Td, the system's temperature only increases by about 35 K from 295 K to 330 K. This relatively small increase in temperature results in only a minor deviation from the initial structure, explaining the observations in Fig. 3. Subsequently, from 100 Td to 200 Td, the temperature increases by about 100K reaching 420 K. The combined mobility data can also be used to obtain a dispersion plot that can then be compared to the raw values of the FAIMS system as observed in Fig. 5.

Fig. 5 presents the outcomes for all three tetraalkylammonium salts. The plot was generated using 120 mobility calculations in total, with 40 dedicated to each of the salts. Reduction coefficients of approximately 1.01 and 1.07 were applied to TDA and THA, respectively, allowing for a fair comparison to the experimental values, as the mobility at the gas temperature is now aligned with experimental values. The results prove quite satisfactory, considering the simplicity of the assumptions and the use of only three candidate structures for each of the salts. While TDA and THA do not precisely match the experimental curve as closely as TDDA, they still imply that the expansion of structures has a notable impact on flexible configurations. We note that the single temperature structure is also displayed here for comparison. This result exhibits a slight variation from that presented in Fig. 3, as it utilizes the MD structure at 295 K (properly reduced) rather than the DFT structure.

Fig. 6 shows the dispersion plots of all three salts, generated using IMoS 1.13, and compares them to their experimental counterparts. To construct these plots, a bisinusoidal wave function $f(t)$ at normalized time values was used for the dispersion field E_d and given by:[9,65]

$$f(t) = \frac{\left(2\sin(\omega t) + \sin\left(2\omega t - \frac{\pi}{2}\right)\right)}{3} \quad (2)$$

with a frequency of ω = 25 Mhz. It is worth noting that the wave function can be customized in IMoS 1.13 using tabulated values if desired to describe a more accurate experimental wave function. For precise dispersion plots, it is crucial to select a significant number of effective temperatures close to the gas temperature. The comparison between the experimental and weighted dispersion plots yields highly satisfactory results, highlighting the method's capabilities while benefiting from fast and optimized trajectory method calculations. It is also quite impossible at this time for machine learning algorithms to reproduce results of structure-varying and high-field calculations.[66–68] Interpreting the results, it is difficult to ascertain the impact of inelasticity on the mobility of polyatomic ions in polyatomic gases at this time. When considering the expansion of structures due to heating, it becomes evident that the contribution of energy directed into the gas's internal degrees of freedom is somewhat less than initially anticipated based on the raw data. It is important to note that ion heating itself represents an inelasticity effect, where energy shifts from translational degrees of freedom to internal degrees of freedom, and this influence can indirectly be embedded within the ξ parameter, as observed in previous work. However, it could be expected that as the ion heats up, it will reach an internal effective temperature that is the same as the translational effective temperature, albeit different than the elastic collision case. The attainment of this equilibrium depends on many variables, including the ion's size, *i.e.*, how many internal degrees of freedom it possesses, and the speed at which the electric field changes. If this internal temperature is reached, closing in essence this mechanism of energy escape, the system will no longer lose energy into the internal degrees of freedom

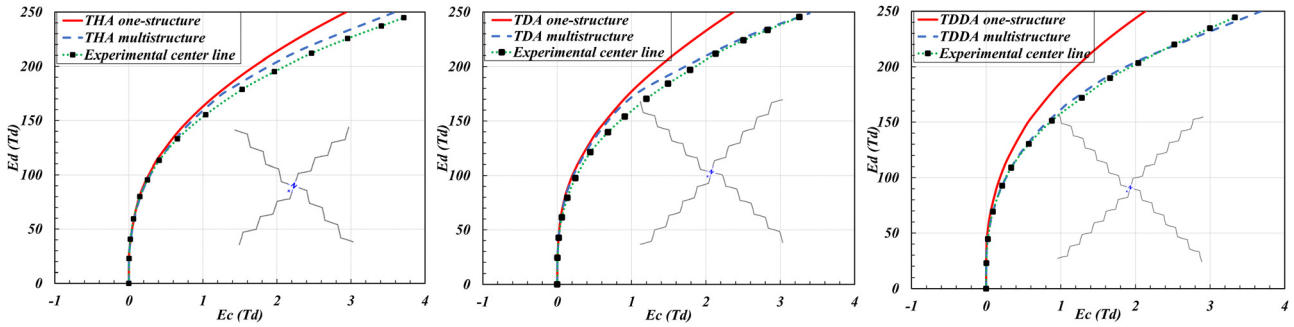

Fig. 6 Dispersion plots show dispersion field (E_d) as a function of compensation field (E_c) for (a) THA, (b) TDA, and (c) TDDA. Shown are the single structure plot, the weighted numerical result, and the experimental raw values.

of the ion. Consequently, the sole mechanism of energy loss will be through the internal degrees of freedom of the gas, primarily involving rotational motion.

While it is conceivable to estimate the energy loss into the internal degrees of freedom of the diatomic gas by adjusting the weighted curve to match the experimental values from Fig. 5, we refrain from pursuing this approach here, given that the results most likely contain errors that are at least of the order of magnitude of the energy loss itself. To conduct this investigation meticulously, it would be prudent to employ molecules with lower flexibility than the alkylammonium salts. However, we suggest that the ions should be large enough that the mobility becomes mostly a strong function of its hard-sphere size and is less dependent on long-range forces. This will limit possible errors from experimental observations and calculations.

Conclusions

In this manuscript, a correction for numerical calculations of the two-temperature theory for flexible salts in diatomic gases and arbitrary fields was attempted and compared to the results obtained using a FAIMS system. As the field increases, the ions are subject to heating from collisions with the gas, increasing their overall temperature to an effective temperature that can be calculated using the two-temperature approximation. However, the two-temperature approximation only considers elastic collisions between monoatomic entities and, as such, a correction must be made for polyatomic entities. In the case of flexible ions such as the long chain tetraalkylammoniums in diatomic gases, we posited that the correction could come from two distinct sources: the enlargement of the ion due to heating and the inelasticity of the collisions where part of the energy goes into the rotational degrees of freedom of the gas molecule.

To assess the impact of these sources, we generated Molecular Dynamic structures using an MM2 forcefield at three distinct temperatures for the three candidate structures, which were modified to match the zero-field mobility. Trajectory methods using these structures were used to calculate mobility as a function of the field using the two-temperature theory up to the fourth approximation in IMoS 1.13. Our computational approach was optimized to calculate only the necessary effective temperatures to create a combined mobility *vs.* reduced field strength plot that uses a linear weighted system.

The results show that the enlargement of the structure has an important contribution to the mobility at high electric fields, and the results obtained using heated structures align better with the experimental data. Dispersion plots were also obtained that exhibit better agreement with the raw data from the FAIMS instrument. The inelasticity from the energy going into the rotational degrees of freedom was not calculated at this time due to its variability and errors associated with its calculation.

Author contributions

V. D. G. and F. M. S.: data curation, formal analysis, investigation, methodology, software, visualization. C. L. A.: conceptualization, formal analysis, funding acquisition, investigation, methodology, project administration, software, supervision, visualization, writing – original draft. All authors: validation, writing – review & editing.

Conflicts of interest

There are no conflicts to declare.

Acknowledgements

We acknowledge the financial support provided by the NSF Division of Chemistry under grant no. 1904879 and 2203968.

References

1 F. Lanucara, S. W. Holman, C. J. Gray and C. E. Eyers, *Nat. Chem.*, 2014, **6**, 281–294.
2 E. A. Mason and E. W. McDaniel, *Transport properties of ions in gases*, John Wiley & Sons, New York, 1988.
3 J. N. Dodds and E. S. Baker, *J. Am. Soc. Mass Spectrom.*, 2019, **30**, 2185–2195.
4 W. A. Donald and J. Prell, *Advances in Ion Mobility-Mass Spectrometry: Fundamentals, Instrumentation and Applications*, Elsevier, 2019.
5 E. A. Mason and H. W. Schamp Jr, *Ann. Phys.*, 1958, **4**, 233–270.

6 G. F. Verbeck, B. T. Ruotolo, K. J. Gillig and D. H. Russell, *J. Am. Soc. Mass Spectrom.*, 2004, **15**, 1320–1324.
7 R. Andrzejewski, A. Entwistle, R. Giles and A. A. Shvartsburg, *Anal. Chem.*, 2021, **93**, 12049–12058.
8 L. A. Viehland and E. Mason, *Ann. Phys.*, 1978, **110**, 287–328.
9 A. A. Shvartsburg, *Differential ion mobility spectrometry: nonlinear ion transport and fundamentals of FAIMS*, CRC Press, 2008.
10 C. P. Harrilal, V. D. Gandhi, G. Nagy, X. Chen, M. G. Buchanan, R. Wojcik, C. R. Conant, M. T. Donor, Y. M. Ibrahim and S. V. Garimella, *Anal. Chem.*, 2021, **93**, 14966–14975.
11 V. D. Gandhi, K. Short, L. Hua, I. Rodríguez and C. Larriba-Andaluz, *J. Aerosol Sci.*, 2022, 106122.
12 W. F. Siems, L. A. Viehland and H. H. Hill Jr, *Anal. Chem.*, 2012, **84**, 9782–9791.
13 V. D. Gandhi and C. Larriba-Andaluz, *Anal. Chim. Acta*, 2021, **1184**, 339019.
14 W. S. Hopkins, in *Comprehensive Analytical Chemistry*, ed. W. A. Donald and J. S. Prell, Elsevier, 2019, vol. 83, pp. 83–122.
15 S. I. Merenbloom, T. G. Flick and E. R. Williams, *J. Am. Soc. Mass Spectrom.*, 2011, **23**, 553–562.
16 C. Ieritano, J. Featherstone, A. Haack, M. Guna, J. L. Campbell and W. S. Hopkins, *J. Am. Soc. Mass Spectrom.*, 2020, **31**, 582–593.
17 V. D. Gandhi, L. Hua, X. Chen, M. Latif and C. Larriba-Andaluz, *Talanta Open*, 2023, **7**, 100191.
18 L. A. Viehland and E. Mason, *Ann. Phys.*, 1975, **91**, 499–533.
19 A. Haack, J. R. Bissonnette, C. Ieritano and W. S. Hopkins, *J. Am. Soc. Mass Spectrom.*, 2022, **33**, 535–547.
20 C. Larriba-Andaluz and J. S. Prell, *Int. Rev. Phys. Chem.*, 2020, **39**, 569–623.
21 G. H. Wannier, *Bell Syst. Tech. J.*, 1953, **32**, 170–254.
22 L. A. Viehland and L. A. Viehland, *Gaseous ion mobility, diffusion, and reaction*, Springer, 2018.
23 L. Viehland, *Swarms of Ions and Electrons in Gases*, Springer, 1984, pp. 27–43.
24 S. Lin, L. Viehland and E. Mason, *Chem. Phys.*, 1979, **37**, 411–424.
25 H. Ellis, E. McDaniel, D. Albritton, L. Viehland, S. Lin and E. Mason, *At. Data Nucl. Data Tables*, 1978, **22**, 179–217.
26 H. Ellis, R. Pai, E. McDaniel, E. Mason and L. Viehland, *At. Data Nucl. Data Tables*, 1976, **17**, 177–210.
27 A. Haack and W. S. Hopkins, *J. Am. Soc. Mass Spectrom.*, 2022, **33**, 2250–2262.
28 V. Gabelica and E. Marklund, *Curr. Opin. Chem. Biol.*, 2018, **42**, 51–59.
29 C. Schaefer, A. T. Kirk, M. Allers and S. Zimmermann, *J. Am. Soc. Mass Spectrom.*, 2020, **31**, 2093–2101.
30 L. Viehland and D. Fahey, *J. Chem. Phys.*, 1983, **78**, 435–441.
31 D. Morsa, V. Gabelica and E. De Pauw, *Anal. Chem.*, 2011, **83**, 5775–5782.
32 A. A. Shvartsburg, F. Li, K. Tang and R. D. Smith, *Anal. Chem.*, 2007, **79**, 1523–1528.
33 P. Aldebert and J. P. Traverse, *J. Am. Ceram. Soc.*, 1985, **68**, 34–40.
34 D. A. Barnett, B. Ells, R. Guevremont, R. W. Purves and L. A. Viehland, *J. Am. Soc. Mass Spectrom.*, 2000, **11**, 1125–1133.
35 V. D. Gandhi, J. Lee, L. Hua, M. Latif, C. J. Hogan and C. Larriba-Andaluz, *Anal. Chem.*, 2023, **95**, 7941–7949.
36 I. Buryakov, *Tech. Phys.*, 2006, **51**, 1121–1126.
37 I. Buryakov, E. Krylov, E. Nazarov and U. K. Rasulev, *Int. J. Mass Spectrom. Ion Processes*, 1993, **128**, 143–148.
38 A. A. Shvartsburg, S. V. Mashkevich and R. D. Smith, *J. Phys. Chem. A*, 2006, **110**, 2663–2673.
39 A. A. Shvartsburg, R. D. Smith, A. Wilks, A. Koehl, D. Ruiz-Alonso and B. Boyle, *Anal. Chem.*, 2009, **81**, 6489–6495.
40 E. O. Knutson and K. T. Whitby, *J. Aerosol Sci.*, 1975, **6**, 443–451.
41 J. Rus, D. Moro, J. A. Sillero, J. Royuela, A. Casado, F. Estevez-Molinero and J. F. de la Mora, *Int. J. Mass Spectrom.*, 2010, **298**, 30–40.
42 V. Shrivastav, M. Nahin, C. J. Hogan and C. Larriba-Andaluz, *J. Am. Soc. Mass Spectrom.*, 2017, **28**, 1540–1551.
43 S. M. Kerwin, *J. Am. Chem. Soc.*, 2010, **132**, 2466–2467.
44 N. L. Allinger, *J. Am. Chem. Soc.*, 1977, **99**, 8127–8134.
45 K. Ohshimo, R. Sato and F. Misaizu, *J. Phys. Chem. A*, 2020, **124**, 7999–8004.
46 G. Paglia, A. J. Smith and G. Astarita, *Mass Spectrom. Rev.*, 2022, **41**, 722–765.
47 J. Wei, Y. Tang, M. E. Ridgeway, M. A. Park, C. E. Costello and C. Lin, *Anal. Chem.*, 2020, **92**, 13211–13220.
48 E. Mucha, A. Stuckmann, M. Marianski, W. B. Struwe, G. Meijer and K. Pagel, *Chem. Sci.*, 2019, **10**, 1272–1284.
49 S. Re, S. Watabe, W. Nishima, E. Muneyuki, Y. Yamaguchi, A. D. MacKerell Jr and Y. Sugita, *Sci. Rep.*, 2018, **8**, 1644.
50 W. Struwe, C. Baldauf, J. Hofmann, P. Rudd and K. Pagel, *Chem. Commun.*, 2016, **52**, 12353–12356.
51 Y. Yamaguchi, W. Nishima, S. Re and Y. Sugita, *Rapid Commun. Mass Spectrom.*, 2012, **26**, 2877–2884.
52 V. D. Gandhi, L. Hua, X. Chen, M. Latif and C. Larriba-Andaluz, *Talanta Open*, 2023, 100191.
53 C. Larriba and C. J. Hogan Jr, *J. Comput. Phys.*, 2013, **251**, 344–363.
54 E. V. Krylov, S. L. Coy and E. G. Nazarov, *Int. J. Mass Spectrom.*, 2009, **279**, 119–125.
55 L. A. Viehland, *Chem. Phys.*, 1994, **179**, 71–92.
56 L. A. Viehland and S. Lin, *Chem. Phys.*, 1979, **43**, 135–144.
57 M. Waldman and E. Mason, *Chem. Phys.*, 1981, **58**, 121–144.
58 J. A. Hornbeck, *Phys. Rev.*, 1951, **84**, 615.
59 J. A. Hornbeck, *Phys. Rev.*, 1950, **80**, 297.
60 A. A. Aksenov and J. T. Kapron, *Rapid Commun. Mass Spectrom.*, 2010, **24**, 1392–1396.
61 J. L. Campbell, M. Zhu and W. S. Hopkins, *J. Am. Soc. Mass Spectrom.*, 2014, **25**, 1583–1591.
62 W. Kohn and L. J. Sham, *Phys. Rev.*, 1965, **140**, A1133–A1138.
63 J. M. McMahon, M. A. Morales, C. Pierleoni and D. M. Ceperley, *Rev. Mod. Phys.*, 2012, **84**, 1607–1653.
64 S. Ude and J. F. de la Mora, *J. Aerosol Sci.*, 2005, **36**, 1224–1237.
65 E. V. Krylov, E. G. Nazarov and R. A. Miller, *Int. J. Mass Spectrom.*, 2007, **266**, 76–85.
66 X. Li, H. Wang, M. Jiang, M. Ding, X. Xu, B. Xu, Y. Zou, Y. Yu and W. Yang, *Molecules*, 2023, **28**, 4050.
67 F. Meier, N. D. Köhler, A.-D. Brunner, J.-M. H. Wanka, E. Voytik, M. T. Strauss, F. J. Theis and M. Mann, *Nat. Commun.*, 2021, **12**, 1185.
68 R. Guo, Y. Zhang, Y. Liao, Q. Yang, T. Xie, X. Fan, Z. Lin, Y. Chen, H. Lu and Z. Zhang, *Commun. Chem.*, 2023, **6**, 139.